Hyperfine structure intervals and absolute frequency measurement in the $2p^4 3s\ ^2P_J \rightarrow 2p^4 3p\ ^2D_{J'}$ fine-structure multiplet of atomic fluorine by diode laser spectroscopy

D. A. Tate and D. N. Aturaliye*
Department of Physics and Astronomy, Colby College, Waterville, Maine 04901
(Received 29 January 1997)

We have measured the hyperfine structure splittings of the three components of the $2p^4 3s\ ^2P_J \rightarrow 2p^4 3p\ ^2D_{J'}$ multiplet in atomic fluorine using both Doppler-free saturated absorption spectroscopy with an external cavity diode laser and Doppler-limited absorption spectroscopy with a noncavity diode laser. Specifically, we have obtained spectra of the $J=1/2 \rightarrow J'=3/2$ transition 780 nm, the $J=3/2 \rightarrow J'=5/2$ transition at 775 nm, and the $J=3/2 \rightarrow J'=3/2$ transition at 761 nm. The fluorine atoms were generated from a 10% mix of F_2 in He using a 2.45-GHz microwave generator and cavity pressures of approximately 0.5 torr. We report here values for hyperfine splittings and constants for the upper and lower states of these transitions. In addition, the absolute frequency of one of the hyperfine components of the $J=1/2 \rightarrow J'=3/2$ transition at 780 nm was measured using a recent absolute frequency measurement of the D_2 transition in Rb. [S1050-2947(97)05509-1]

PACS number(s): 32.10.Fn, 32.30.Jc

I. INTRODUCTION

Historically, laser spectroscopy of the nonmetallic elements in periods 2 and 3 of the Periodic Table has been a relatively unexplored field. The principal reasons for this are that the resonance transitions of these atoms lie in the ultraviolet region and also the natural states of such atoms are either diatomic molecules (e.g., N_2, O_2, and F_2) or macromolecules (e.g., C, Si, and S). However, many of the transitions between excited states of these atoms lie in the visible and near infrared and can be driven using $Ga_{1-x}Al_xAs$ or $In_zGa_{1-y}Al_yP_{1-z}$ diode lasers. Consequently, there has been a substantial amount of progress in recent years in making measurements of hyperfine structure (hfs) intervals and isotope shifts in atomic oxygen [1,2] and nitrogen [3], using diode lasers. These measurements are of interest since experimental values for hyperfine structure constants and isotope shifts are quantities that depend on the electron wave function close to the nucleus and serve as a stringent test for theoretical predictions for these wave functions. For instance, recent isotope shift measurements in O have revealed a volume shift contribution, unusual in such a light atom, which has been attributed to the doubly magic number of nucleons in the ^{16}O nucleus [4].

The halogens are important in many chemical processes and for this reason there has been interest in the possibility of laser remote detection of these species in both their molecular and atomic forms [5–7]. Obviously, remote detection relies on the fact that the spectrum of the species one wishes to detect is well known and hence spectral studies of such species are important. The study reported in this paper concerns atomic fluorine, a very reactive free radical for which the high-resolution spectrum is not well known. It has only one stable isotope, ^{19}F, with nuclear spin $I=\frac{1}{2}$, thus making its hyperfine spectrum relatively straightforward to interpret. However, the poisonous and corrosive nature of molecular fluorine has resulted in relatively few studies of this species. Stanton and Kolb [5] and Laguna and Beattie [6] measured the hfs intervals of the $2p^5\ ^2P_{3/2} \rightarrow {}^2P_{1/2}$ states using mid-infrared diode lasers. In addition, Herring *et al.* [7] have measured excited-state lifetimes and quenching rates. However, the two most recent papers in which measurements of excited-state hfs splittings are reported are those of Lidén [8] in 1949 and Hocker [9] in 1978. Lidén used grating and interferometric techniques to measure the absolute frequencies of a large number of transitions in atomic fluorine from the ultraviolet to the infrared, some of which had resolvable hfs at the resolution limit of the étalon used for these experiments. Hocker measured the hfs intervals of a number of transitions in the near infrared associated with laser emission from an excited helium-fluorine mixture using a 10.9-m echelle spectrograph.

In the present paper, we report on the measurement and analysis of hyperfine structure intervals of the $3s\ ^2P_J \rightarrow 3p\ ^2D_{J'}$ fine structure multiplet components at 761, 775, and 780 nm, which have been investigated previously by both Lidén and Hocker. [Throughout this paper, we adopt the convention that unprimed angular momentum quantum numbers (J,F) refer to the lower-energy level and primed quantities (J',F') refer to the upper level.] This is the first time, to our knowledge, that high-resolution laser spectroscopy has been performed on excited states of atomic fluorine.

Excited states of atomic fluorine were efficiently excited from molecular fluorine using a microwave discharge [10] and helium as a buffer gas. Spectra of the transitions were obtained using a tunable external cavity diode laser [11,12]. The Doppler-limited and Doppler-free spectra were fitted to obtain the natural linewidths and hfs splittings within a given fine structure multiplet.

*Present address: School of Environmental Science, Engineering and Policy, Drexel University, Philadelphia, Pennsylvania 19104.

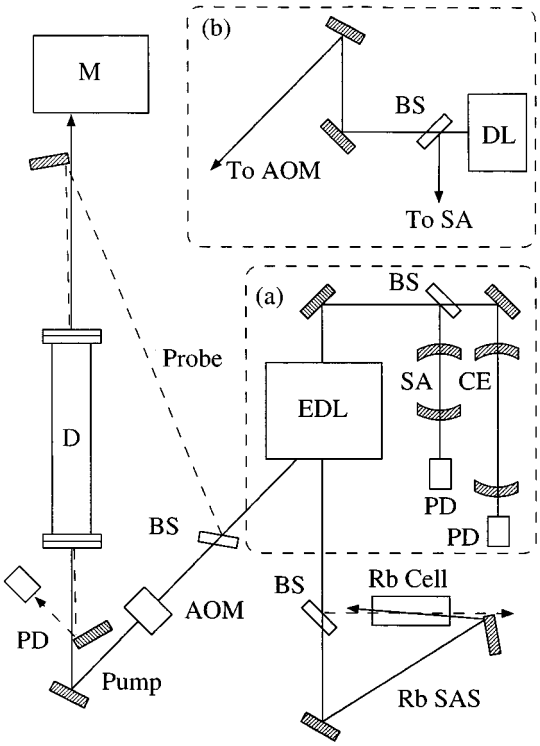

FIG. 1. Experimental apparatus for saturated absorption spectroscopy of fluorine: EDL, external cavity diode laser; DL, nonexternal cavity diode laser; PD, photodiode; SA, 2-GHz confocal spectrum analyzer; CE, 150-MHz confocal étalon; BS, beam splitter; AOM, acousto-optic modulator; *D*, F/He microwave discharge tube; *M*, 0.275-m monochromator; Rb SAS, rubidium saturated absorption spectrometer. For the spectra at 780 and 775 nm, the external cavity diode laser shown in (a) was used. At 761 nm, the noncavity diode laser shown in (b) was used.

II. EXPERIMENTAL METHOD

The experimental apparatus used in this work is shown schematically in Fig. 1. Two diode laser systems were used to obtain the Doppler-free and Doppler-limited spectra. The transitions at 780 nm ($3s\ ^2P_{1/2}\rightarrow 3p\ ^2D_{3/2}$) and 775 nm ($3s\ ^2P_{3/2}\rightarrow 3p\ ^2D_{5/2}$) were observed using a Sharp LT024 30-mW diode laser in a temperature stabilized external cavity [11,12]. One end of the cavity was formed by a 1200-line/mm blazed grating mounted on a commercial mirror mount; a thin piezoelectric disk mounted behind one of the adjustment screws allowed for fine tuning of the laser frequency. Coarse laser frequency adjustments were made by changing the laser injection current and the baseplate temperature and using the mirror mount adjustment screws. The laser was enclosed within a sealed aluminum box. In addition to the output beam from the grating, four other, weaker beams were split out of the cavity using an uncoated glass plate; all the laser beams exited the laser enclosure via microscope slide windows. The laser frequency was scanned with a sawtooth voltage ramp applied to the piezoelectric disk. Using this method we were able to scan the laser over a range of up to 10 GHz, with the laser jitter being of order ± 1 MHz. The strongest output beam had a power of ≈ 5 mW.

The main beam from the laser grating was used for the fluorine saturated absorption spectrometer. The Doppler-free absorption signal was observed using standard saturated absorption techniques with an acousto-optic modulator (AOM) (IntraAction Corporation) and lock-in amplifier (Stanford Research Systems). An uncoated glass window split off $\approx 10\%$ of the laser power for the probe beam. The pump beam power was sinusoidally ''chopped'' at 4 kHz with a 50% duty factor by modulation of the 47.98-MHz AOM drive signal. (In the configuration used, the first-order diffracted beam from the AOM was used as the pump beam and was downshifted by 47.98 MHz with respect to the diode laser frequency.) The pump and probe beams crossed within the discharge tube (described below) at an angle of 7.5 mrad. The probe beam was detected using a photodiode (UDT Sensors) and the Doppler-free signal was recovered by the lock-in amplifier using the AOM chopping frequency as reference. Neither the pump nor the probe beam was focused; the average pump beam laser power entering the discharge tube was 1 mW (2 mW before the AOM) and the laser spot size was approximately 0.5×1.0 mm^2. One of the beam from the laser intracavity beam splitter was used to monitor the laser mode structure using a 2-GHz confocal étalon (Tek Optics) and also to calibrate the frequency scan using a temperature stabilized 150-MHz free spectral range confocal étalon (Burleigh Instruments).

One of the other beams from the beam splitter was used in a rubidium saturated absorption spectrometer. The Doppler-free rubidium spectrum was used to make a precise determination of the 150-MHz étalon free spectral range using the well-known hfs splittings of Rb at 780 nm [13]. Using this method, the étalon's free spectral range was found to be 150.127 ± 0.022 MHz. Repetitive scans of the Rb spectrum taken at 5 min intervals revealed that the cavity drift rate was of the order of a few megahertz per minute. However, since the data scans were taken in a time of 20 s, this drift was negligible (<1 MHz) within any one scan. In some of our measurements, where it was necessary to measure a frequency interval between spectral features in two different scans taken at intervals of 2–5 min, we were careful to alternate scans between the two features several times so we could subtract off the drift of the étalon. The rubidium spectrum was also used to make a determination of the absolute frequency of one of the F hyperfine transitions, as described below. The laser was tuned close to the appropriate frequency of the $2p^4 3s\ ^2P_J\rightarrow 2p^4 3p\ ^2D_{J'}$ transitions [14] using a 0.275-m monochromator (Acton Research Corporation).

We were unable to pull the Sharp laser diode frequency to 761 nm to observe the $3s\ ^2P_{3/2}\rightarrow 3p\ ^2D_{3/2}$ transition using the external cavity. Consequently, the transition at 761 nm could only be observed with a nonexternal cavity, temperature, and injection current stabilized diode laser (Mitsubishi ML4405), mounted in a commercial mount (ILX Laser Corporation). The laser power was 3 mW and the effective laser linewidth approximately 50 MHz (estimated using the 2-GHz spectrum analyzer). The laser frequency was scanned by ramping the injection current at a frequency of either 0.02 Hz (25-s scan) or 20 Hz (25-ms scan), with a maximum scan amplitude of approximately 20 GHz. These spectra were calibrated using the 2-GHz free spectral range confocal étalon (Tek Optics). (The free spectral range of the étalon was

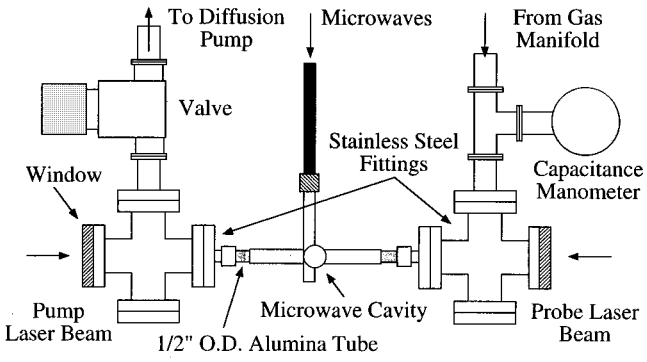

FIG. 2. Diagram of the F_2/He microwave discharge system for producing excited states of F.

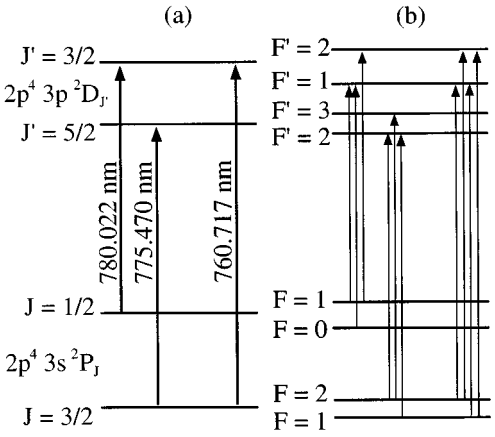

FIG. 3. Partial term diagram of F showing the states investigated in this work. In (a) the gross structure of the $2p^4 3s\ ^2P_J$ and $2p^4 3p\ ^2D_{J'}$ states is shown. The $^2P_{3/2}$ state lies 104 732 cm^{-1} above the ground state of F, $^2P_{1/2}$ at 105 057 cm^{-1}, $^2D_{5/2}$ at 117 624 cm^{-1}, and $^2D_{3/2}$ at 117 874 cm^{-1}. In (b) the effect of the hyperfine interaction is shown, assuming that the hfs is noninverted. Also shown are the relative positions of the various hf components of the transitions.

also calibrated using the Rb Doppler-free spectrum at 780 nm and found to be 1997.7±0.3 MHz.) Observation of the 2-GHz étalon fringes revealed that the laser frequency scan was somewhat nonlinear, though we were able to remove most of this using the spectrum analyzer fringes to linearize the spectra. The inherent low power of this laser and the relative weakness of the 761-nm component restricted us to observing the Doppler-limited spectra of this transition. These spectra were required to confirm our assignments of the total angular momenta (F,F') of the upper and lower states of the 775- and 780-nm transitions since the 761-nm transition shares its lower state with the 775-nm transition $(J=3/2)$ and its upper state with the 780-nm component $(J'=3/2)$.

The spectra were acquired using a digitizing oscilloscope (Tektronix) and transferred to a personal computer (PC). The raw data were then transferred to a Macintosh Power PC and analyzed using a commercial software package. The typical analysis procedure involved linearizing the spectra using the étalon fringes and then fitting the Voigt profiles to obtain line centers and homogeneous widths, and any Gaussian background features due to collisions.

Excited fluorine atoms are generated from a 10% mix of F_2 in He (premixed excimer laser gas from Matheson) in a low-pressure (~0.25–4 torr) microwave discharge. A diagram of the discharge system is shown in Fig. 2. The system was comprised of a gas manifold, discharge region, optical access for the lasers, and a pump. The vacuum system was evacuated using a 4-in. diffusion pump and the pressure in the discharge was measured using a capacitance manometer (MKS Instruments). The discharge region of the vacuum system was formed from a $\frac{1}{2}$-in.-diam, 12-in.-long alumina tube (McMaster Carr) that was coupled to the rest of the system via O-ring flanges. Most of the other parts of the vacuum system were fabricated from standard stainless-steel components (MDC). The system was configured so that gas was pumped through the alumina tube from the gas bottle and regulators to the pump. High-quality quartz windows were O-ring sealed onto the vacuum system so as to allow the laser beams to pass longitudinally through the 6-in-long discharge region. A McCarroll-type microwave cavity (Opthos Instruments) was attached to the outside of the alumina tube; up to 120 W of microwave power at 2.45 GHz was coupled into the cavity by a coaxial cable. Two adjustment screws on the cavity allowed optimization of the coupling and cavity resonance frequency. The alumina tube was cooled using compressed air. Our initial studies were carried out with a Pyrex discharge tube, which rapidly degraded due to the action of excited fluorine and helium atoms. The alumina tube showed no discernible damage in several months' use. The quartz windows remained optically clear long enough to complete the experiment.

This system allowed us to generate excited states of atomic fluorine efficiently through the well-known excitation mechanism of collisional pumping by metastable helium atoms [15]. Optimum conditions of signal to noise while minimizing pressure broadening and rf power broadening were achieved with between 20 and 40 W of microwave power and at between 0.5 and 1.0 torr total pressure (between 0.05 and 0.1 torr partial pressure of F_2) Many spectra were taken of each transition at various laser powers, microwave powers, and pressures so that the zero pressure and zero power widths and splittings could be determined by extrapolation.

III. RESULTS AND DISCUSSION

We discuss the data in the following three sections. First, we present the $^2P_{1/2}\rightarrow{}^2D_{3/2}$ (780 nm) and $^2P_{3/2}\rightarrow{}^2D_{5/2}$ (775 nm) data and second the $^2P_{3/2}\rightarrow{}^2D_{3/2}$ (761 nm) data. Finally, we describe our measurement of the absolute frequency of the $^2P_{1/2}(F=1)\rightarrow{}^2D_{3/2}(F'=2)$ transition.

A. The $^2P_{1/2}\rightarrow{}^2D_{3/2}$ and $^2P_{3/2}\rightarrow{}^2D_{5/2}$ transitions

A term diagram of the $2p^4 3s\ ^2P_J\rightarrow 2p^4 3p\ ^2D_{J'}$ fine structure transition multiplet is shown in Fig. 3. Figure 3(a) shows the fine structure (that is, ignoring the hfs) and transition wavelengths obtained from tables [14]. (For reference, the $^2P_{3/2}$ state lies 104 732 cm^{-1} above the ground state of F, $^2P_{1/2}$ at 105 057 cm^{-1}, $^2D_{5/2}$ at 117 624 cm^{-1}, and $^2D_{3/2}$ at 117 874 cm^{-1}.) Figure 3(b) shows the expected relative positions of the hf states, assuming that the hfs is noninverted, and the expected hfs components of the three fine structure transitions. The $^2P_{1/2}\rightarrow{}^2D_{3/2}$ (780 nm) and

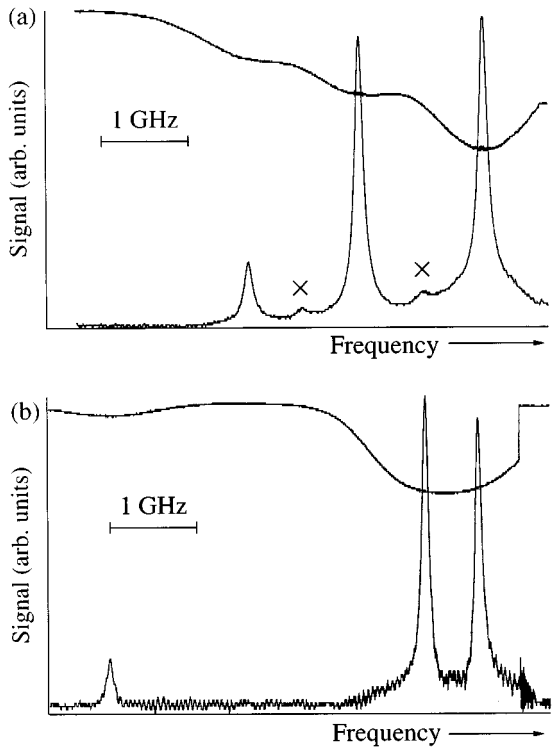

FIG. 4. Doppler-limited and Doppler-free spectra of the (a) $J=1/2\rightarrow J'=3/2$ transition at 780 nm and the (b) $J=3/2\rightarrow J'=5/2$ transition at 775 nm. In each case, the upper (inverted) trace is the Doppler-limited spectrum and the lower trace is the saturated absorption spectrum. Discontinuities at the high-frequency ends of both spectra are due to diode laser mode hops. Note that the scans at the two different wavelengths were taken under different conditions of pressure and microwave power, resulting in a different signal-to-noise ratio and collisional broadening. In the Doppler-free spectrum of (a), the two small features (labeled $\times$) are collision-induced crossovers.

$^2P_{3/2}\rightarrow{}^2D_{5/2}$ (775 nm) transitions each have three hyperfine (hf) components, while the $^2P_{3/2}\rightarrow{}^2D_{3/2}$ (761 nm) line has four hf components.

Figures 4(a) and 4(b) show examples of the spectrum of the $^2P_{1/2}\rightarrow{}^2D_{3/2}$ and $^2P_{3/2}\rightarrow{}^2D_{5/2}$ transitions, respectively. The upper trace in Fig. 4(a) is the Doppler-limited spectrum at 780 nm (this is actually the laser power transmitted through the fluorine discharge, hence the inverted features; typically, 20–30% of the incident laser power was absorbed in the discharge). The expected three hf components are separated by greater than their Doppler width; the lower trace in Fig. 4(a) is the corresponding saturated absorption spectrum. The two smaller features are collision-induced crossovers and are discussed below. The upper trace in Fig. 4(b) is the Doppler-limited spectrum at 775 nm. There are two main features: a weak absorption and a much stronger and broader feature some 5.6 GHz higher in frequency. The lower trace in Fig. 4(b) is the Doppler-free saturated absorption spectrum, which shows that the broad strong feature in the Doppler-limited spectrum actually has two components separated by less than the Doppler width. Hence, at 775 nm, there are three hf components to the spectrum, as expected. [There are diode laser mode hops at the high-frequency ends of the spectra in both Figs. 4(a) and 4(b), leading to the apparent discontinuity of the Doppler-limited spectrum in Fig. 4(a) and the sharp cutoff in the Doppler-limited spectrum in Fig. 4(b). The difference in the signal-to-noise ratio apparent in these two scans is due to different conditions of pressure and microwave power.] We found the optimum signal-to-noise conditions were obtained at a total pressure of 0.6 torr (i.e., a partial pressure of 0.06 torr of F_2), with a microwave power of 20–40 W depending on the transition under study. To find the hfs splittings and transition linewidths, we made measurements at pump beam powers between 0.1 and 1 mW, pressures between 0.25 and 4.0 torr, and microwave powers between 20 and 100 W. There were relatively strong linewidth dependences on laser power and discharge pressure, but negligible dependence on the microwave power.

As mentioned above, the frequency scale of the raw data was linearized using the 150-MHz étalon fringes. The Doppler-free spectra were then fitted to Voigt profiles to find the Lorentzian widths and relative positions of the components. At higher pressures (above approximately 1 torr), Doppler-broadened pedestals on the stronger peaks became apparent and crossover resonances appeared between the two stronger features at 775 nm and between all three components at 780 nm. In all cases the crossovers were weak ($<5\%$ of the maximum transition amplitude) and appeared in their expected positions. In fitting the Voigt profiles, the positions, amplitudes, and Lorentzian widths of each component were free parameters, together with a background offset and slope. The Gaussian full width at half maximum (FWHM) widths were fixed to 13 MHz, the value expected for the residual Doppler broadening due to the nonzero crossing angle of the pump and probe beams. This value was calculated from the Doppler widths at 761 nm (1.7 GHz FWHM; see below) and the measured pump-probe beam crossing angle of 7.5 mrad [16]. In the high-pressure scans, we also added Gaussian backgrounds to the stronger peaks and crossovers with floating amplitudes, but positions fixed at the mean frequency of pairs of allowed transitions. Examples of the fits are shown in Fig. 5: Fig. 5(a) shows the experimental and fitted spectra at 780 nm and Fig. 5(b) shows the experiment and fit at 775 nm. In both diagrams, the upper trace is the residual difference between the experiment and the fit. As can be seen, there appear to be no systematic deviations from the fit once the Doppler backgrounds and crossovers have been included at levels of greater than 2% of the maximum signal amplitude. Even though the Lorentzian widths of each of the three components at each wavelength were free parameters in the fits, the widths of the two strongest peaks at each wavelength agreed within 5%, though the weakest peak in each of the spectra was usually somewhat wider as a result of a poorer signal-to-noise ratio.

The measurements of the spectra as the pressure and laser power are extrapolated to zero give a natural linewidth of $\gamma=114\pm12$ MHz, where the error is to be understood as a standard deviation. This number is an average of the widths of the two strongest peaks at each wavelength (780 and 775 nm) and was obtained using data from a total of 50 data scans. From these data, we found that the FWHM widths of the components were broadened by 12 MHz/torr at 780 nm and 34 MHz/torr at 775 nm. In addition, the estimated broad-

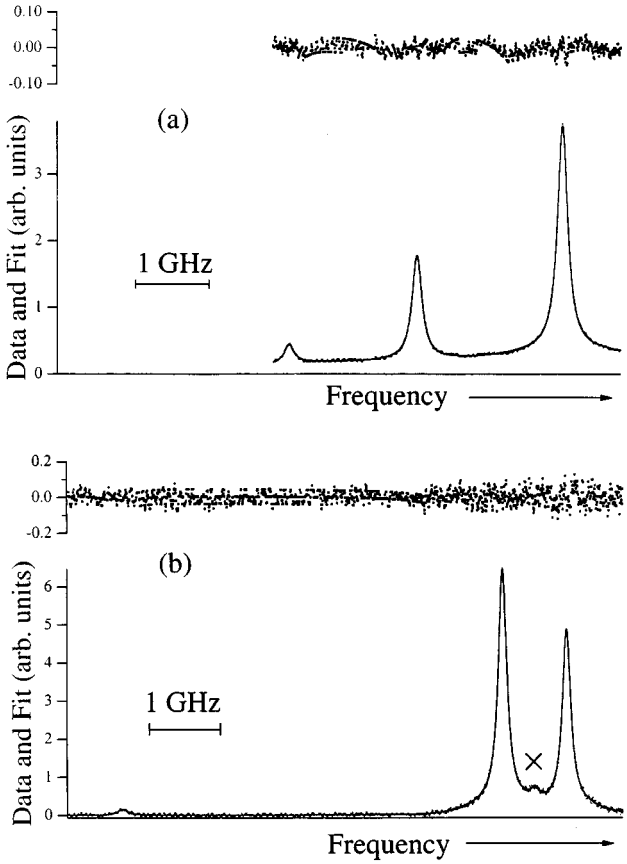

FIG. 5. Fits of the Doppler-free spectra at (a) 780 nm and (b) 775 nm, together with the residuals (data minus fit) shown above the spectra. The vertical axis for the residuals has the same scale as that for the data and fit. Note that the crossover resonances shown in the Doppler-free spectrum of Fig. 4(a) are absent here since the discharge pressure and microwave power were higher in Fig. 4(a) than here. In (b) there is a crossover resonance (labeled ×), which was absent in Fig. 4(b) as the pressure and power are higher here than in Fig. 4(b).

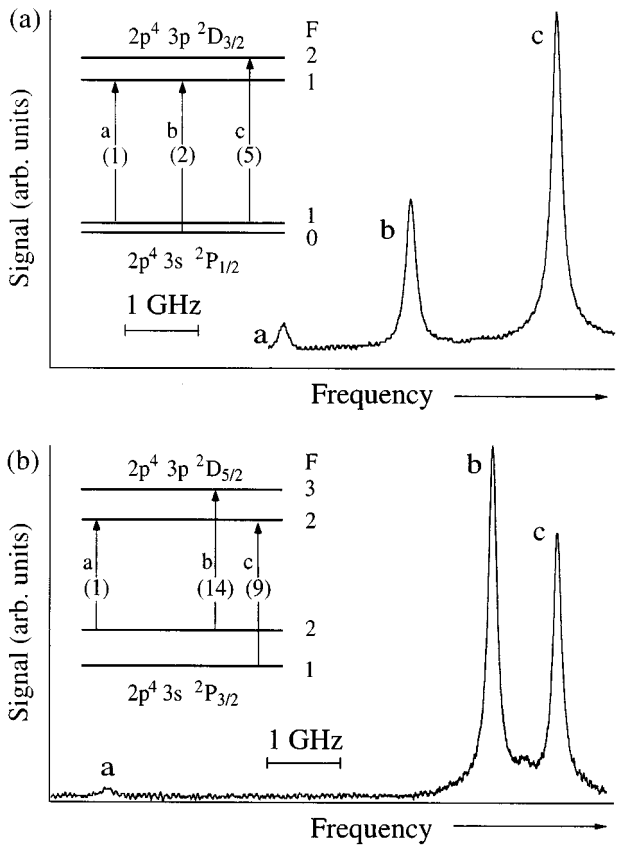

FIG. 6. Data scans of Fig. 5 at (a) 780 nm and (b) 775 nm, shown together with diagrams of the hfs in the lower and upper states (assumed to be normal), the allowed hf transitions, and the expected relative intensities. Within each spectrum, the labels a, b, and c each represent the F values connected by a particular hf component: for instance, in (a), a represents the $F=1\rightarrow F'=1$ component, as shown in the hfs diagram of (a). The same labels are assigned to the three features in the spectra on the basis of their relative intensities.

ening due to laser power under the operating conditions we used (i.e., an average pump laser power of 1 mW) was 16 MHz in the full width at half maximum. We can compare the value for γ we obtained with that expected from knowledge of the known lifetimes of the upper and lower levels,

$$\gamma=\left(\frac{1}{2\pi}\right)\left(\frac{1}{\tau_u}+\frac{1}{\tau_l}\right).$$

The lifetime of the lower $3s\ ^2P_J$ level is $\tau_l=1.28\pm0.07$ ns [17] and the lifetime of the upper $3p\ ^2D_{J'}$ level is $\tau_u=27\pm1$ ns [7]. Using these values, we obtain the value $\gamma=130\pm7$ MHz, in reasonable agreement with our experimental result.

In addition to the linewidths, we were able to compare the relative transition amplitudes of the hfs components at each wavelength. In Fig. 6, we again show the experimental spectra of Fig. 5, together with the expected positions of the upper and lower hfs states, assuming that the hfs in both states is normal (i.e., noninverted). One can estimate the relative amplitudes of the hf components using the Ornstein-Burger-Dorgelo sum rule. At 780 nm [Fig. 6(a)], the relative amplitudes of the a, b, and c components (in order of increasing frequency) are expected to be 1:2:5 (0.20:0.40:1.0), whereas we actually observe the approximate ratio 0.08:0.44:1.0 under conditions that give an optimum signal-to-noise ratio, though this changes somewhat depending on the discharge conditions. At 775 nm [Fig. 6(b)], the expected ratio of the a, b, and c component intensities is 1:14:9 (0.07:1.0:0.64) and we observe 0.03:1.0:0.75. At both 780 and 775 nm, the a components are somewhat less strong than expected, though they increased somewhat relative to the b and c lines as the microwave power to the discharge was increased. This phenomenon is presumably due to the large Doppler-limited absorption of the pump and probe beams, which reduces the laser power in the region where they overlap and also reduces the power transmitted to the detector. For instance, in the Doppler-limited spectra shown in Fig. 4, the amplitudes of the hyperfine components conform more closely to their expected ratios. At high pressures (above 1 torr) the b and c components in the Doppler-free spectra at both 780 and 775 nm tended to the same relative amplitudes.

As noted above, at higher pressures and microwave pow-

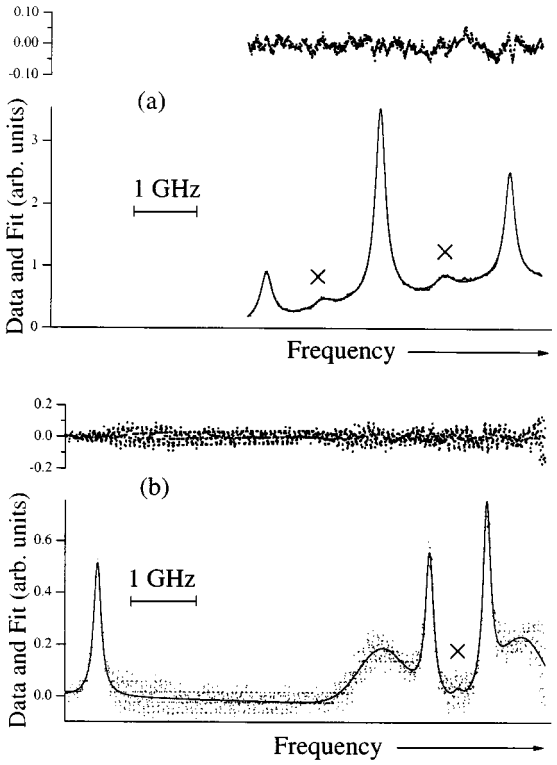

FIG. 7. Data scans at higher pressure and microwave power. In (a), a spectrum at 780 nm is shown, taken at 95 W microwave power and 3.9 torr pressure. In (b), a spectrum at 775 nm is shown, taken at 60 W and 0.9 torr. Crossovers are labeled ×.

ers, the saturated absorption profiles tended to broaden and their relative amplitudes changed. In addition, at 780 nm, Doppler-broadened pedestals appeared beneath the three hf components and crossover resonances also appeared. An example of this is shown in Fig. 7(a), where the spectrum shown was obtained at 95 W of microwave power and 3.9 torr total pressure. As can be seen, the *b* component is now stronger than the *c* component. To fit this spectrum, it was necessary to add three Gaussian pedestals of equal widths, centered on the positions of the hf transitions, and three crossovers at the average frequencies of pairs of ''real'' transitions (one of these lies in the high-frequency wing of the central *b* peak). The Doppler pedestals have widths of 1.9 GHz FWHM, corresponding to a discharge temperature [18] of approximately 900 K, and are caused by velocity-changing collisions [19]. These velocity-changing collisions are responsible for the appearance of the crossovers, which do not occur at lower pressures because the hf features are separated by more than the Doppler width, and also the crossover resonance midway between features *b* and *c*, which have neither a lower level nor an upper level in common [20].

In contrast, the higher-pressure spectra at 775 nm show a different behavior. Again, there is a crossover between *b* and *c* (which have no level in common), apparent at relatively low pressures, and both *b* and *c* have Doppler pedestals, which were included in the fit of Fig. 5(b). However, at higher pressures, another interesting feature arises, namely, the evolution of the Doppler pedestals centered on *b* and *c* to

TABLE I. Experimental values of the hyperfine structure splittings of the $3s\ ^2P_{1/2}$, $3s\ ^2P_{3/2}$, $3p\ ^2D_{3/2}$, and $3p\ ^2D_{5/2}$ states.

Level	$F,F-1$	$\Delta_{F,F-1}$ (MHz)		
		This work	Ref. [8]	Ref. [9]
$3s\ ^2P_{1/2}$	1,0	1737.1±4.0	180±150	2130±550
$3s\ ^2P_{3/2}$	2,1	6115.7±4.1	4590±150	5400±550
$3p\ ^2D_{3/2}$	2,1	3714.3±4.2	3060±150	−4050±550
$3p\ ^2D_{5/2}$	3,2	5239.6±4.5	5250±150	−1500±550

two relatively narrow Gaussians (880 MHz FWHM) positioned on either side of the *b*-*c* doublet. This phenomenon, shown in Fig. 7(b) (data taken at 60 W microwave power and 0.9 torr pressure), is possibly due to nonthermal velocity distributions in the upper and lower states of this transition multiplet. Such a mechanism has been hypothesized for the laser emission at 780 nm, 775 nm, and other near-infrared wavelengths from an excited helium-fluorine mix, as described in Ref. [9] and the references therein. In this model, dissociation a repulsive state of the HeF excimer preferentially populates the $3p\ ^2D_{J'}$ states. An inherent consequence of this population by dissociation mechanism is that atoms in the $3p\ ^2D_{J'}$ states have a much higher temperature (and thus a wider velocity distribution) than the $3s\ ^2P_J$ states. In addition, the effective lifetime of the $3s\ ^2P_J$ states is relatively long because of radiation trapping of the $2p^4 3s\ ^2P \rightarrow 2p^5\ ^2P$ resonance radiation in the optically dense discharge. Consequently, laser emission is only possible in the high- and low-frequency wings of the $3s\ ^2D_{J'} \rightarrow 3s\ ^2P_J$ transition for velocity classes of atoms where the upper state population exceeds that of the lower state. This model was first applied to the $2p^3 3p\ ^3P_{0,1,2} \rightarrow 2p^3 3s\ ^3S_1$ laser transition in atomic oxygen at 845 nm [21]. Such a model may explain why the anomalous features appear at lower and higher frequencies than the ($F=2 \rightarrow F'=3$) and $F=1 \rightarrow F'=2$) components of the $^2P_{3/2} \rightarrow\ ^2D_{5/2}$ transition at 775 nm, but if so, it is unclear why we only observe symmetric Doppler pedestals in the $^2P_{1/2} \rightarrow\ ^2D_{3/2}$ transition at 780 nm, which is also a transition in which laser emission has been reported. We intend to pursue this question in a subsequent investigation.

On the basis of the relative intensities of the hf components at both 780 and 775 nm we concluded that the hfs splittings of both the $3s\ ^2P_J$ and $3p\ ^2D_{J'}$ states are normal and that the *a*, *b*, and *c* components at each wavelength correspond to the transitions between the hfs levels shown in the insets in Figs. 6(a) and 6(b). It is then straightforward to obtain the splittings between the various *F* levels of the upper and lower states, and these quantities are given in Table I. The values in the table are obtained from approximately 18 spectra at each of the two wavelengths (780 and 775 nm), taken at various discharge pressures. The splittings are obtained from extrapolation to zero pressure and the quoted errors are one standard deviation of the results. Also included in Table I are the hfs splittings obtained from Refs. [8] and [9]. In this table, the uncertainties quoted for the previous values of the hfs intervals are estimated in the following manner. Lidén [8] estimates the uncertainties of his measurements of the hfs intervals to be between 0.002 and 0.005 cm^{-1}; we have used 150 MHz, corresponding to the larger

TABLE II. Magnetic dipole hfs constants (A) for the $3s\ ^2P_{1/2}$, $3s\ ^2P_{3/2}$, $3p\ ^2D_{3/2}$, and $3p\ ^2D_{5/2}$ levels.

Level	A (MHz)
$3s\ ^2P_{1/2}$	1737.1±4.0
$3s\ ^2P_{3/2}$	3057.9±2.1
$3p\ ^2D_{3/2}$	1857.1±2.1
$3p\ ^2D_{5/2}$	1746.5±1.5

uncertainty limit, in Table I. Hocker [9] estimates his resolution to be about 1 part in 700 000, or an uncertainty of about 550 MHz for the hfs intervals in this region of the infrared. As can be seen, our data are much more precise than in either of the previous works and there are significant differences between some of our hfs splittings and those of Refs. [8] and [9], which also do not agree with each other in three out of the four values given. Lidén's value of the hf splitting of the $^2D_{5/2}$ state is in good agreement with ours, though the agreement for the $^2D_{3/2}$ and $^2P_{3/2}$ states is good to only 20–30%, well outside his error limits, and for $^2P_{1/2}$, there is an even larger discrepancy. However, Lidén could resolve no hfs splitting in the transition at 775 nm and could resolve only two of the three hfs components at 780 nm and two of four components at 761 nm. It is therefore not clear whether his observation of a given fine structure transition splitting corresponds to the lower- or upper-state hf splitting or a linear combination of the two. Presumably, he was able to extract the $3s\ ^2P_J$ and $3p\ ^2D_{J'}$ hf intervals from the 780-, 775-, and 761-nm data in conjunction with his measurements of the hfs splittings of other transitions to and from these levels (the $3p\ ^2P_J \rightarrow 3s\ ^2P_J$, $3p\ ^2S_J \rightarrow 3s\ ^2P_J$, and $4d\ ^4F_J \rightarrow 3p\ ^2D_J$ multiplets) and estimate the maximum splittings of the unresolved multiplets. It is thus perhaps not so surprising that the agreement between our results and Lidén's is relatively poor. Hocker's data, on the other hand, are in reasonable agreement with ours for the $^2P_{1/2}$ and $^2P_{3/2}$ states, at his experimental uncertainty. However, his values for the splittings of the $^2D_{3/2}$ and $^2D_{5/2}$ states are negative, implying an inverted hfs, and the magnitudes of the splittings are significantly different from ours. The most probable reason for this discrepancy is that Hocker observed the transitions in light emitted from a laser cavity whose length was tuned to be resonant with each emission line in turn. Hocker found that the number of resolvable components of each laser line did not correlate well with the number of expected hf components. In addition, the laser action can seriously change the relative transition strengths and, as we have seen, the proposed mechanism for laser action implies that stimulated emission can occur at a frequency that may be as much as several hundred megahertz away from the line center and also that one transition can give rise to two laser emission frequencies [21].

Using the splittings tabulated in Table I, the magnetic-dipole hyperfine coupling constants A can be obtained. (Since, for ^{19}F, $I=\frac{1}{2}$, the nucleus is spherically symmetric and the electric-quadrupole coupling constant B is equal to zero [22].) Using Landé's formula, in the case of no electric-quadrupole coupling, the frequency splitting between two adjacent hyperfine levels with F values that differ by one is

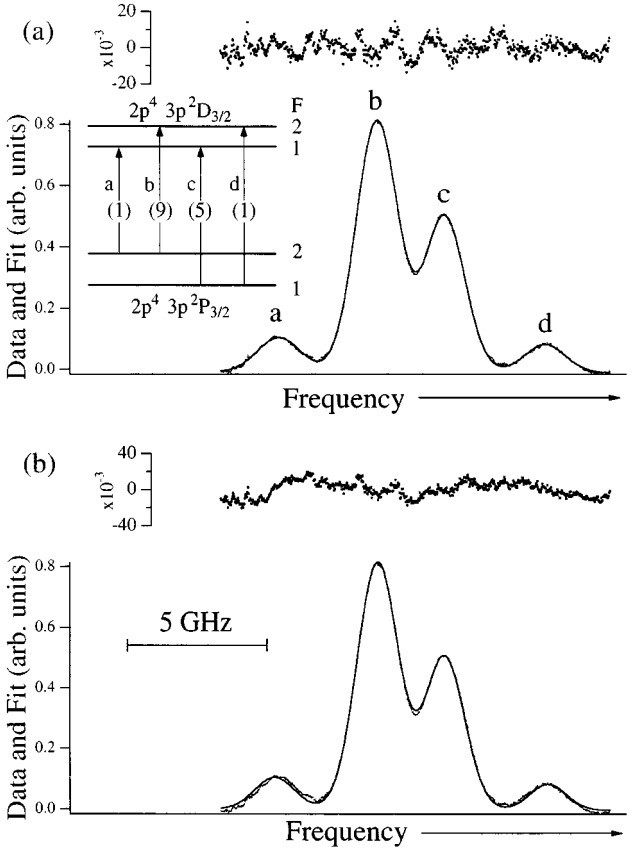

FIG. 8. Fits of the Doppler-limited $J=3/2 \rightarrow J'=3/2$ spectra at 761 nm. In (a) the data and fit are shown when the positions of the four components are free parameters, with the residuals shown above with the same relative scaling. Also shown in (a) is the hfs of the lower and upper states (assumed normal), the allowed hf transitions, and their relative intensities. The labels, a, b, c, and d each represent the F values connected by a particular hf component: for instance, a represents the $F=2 \rightarrow F'=1$ component, as shown in the hfs diagram. The same labels are assigned to the four features in the spectra on the basis of their relative intensities. In (b), the data, fit, and residuals are shown when the relative positions of the four hf components are fixed using the values for the hfs coupling constants obtained from the spectra at 780 and 775 nm. Note the change in the frequency scale from that of Figs. 4–7 and also the change in the residuals scale between (a) and (b).

$$\Delta_{F,F\text{-}1} = A_{\alpha J} F,$$

where J is the total electronic angular momentum and α represents all the other quantum numbers necessary to specify completely the fine structure level in question. Hence it is easy to obtain the magnetic-dipole coupling constants $A_{\alpha J}$. The values of these quantities obtained from our experiments are given in Table II.

B. The $^2P_{3/2} \rightarrow {}^2D_{3/2}$ transition

In order to confirm that the F labels we assigned to the hf levels shown in Fig. 6 were correct, we also obtained spectra of the $^2P_{3/2} \rightarrow {}^2D_{3/2}$ transition at 761 nm. This transition shares its lower state with the 775-nm transition and its upper state with the 780-nm transition, as shown in Fig. 3. The

expected four components are visible in the Doppler-limited spectrum, as seen in Fig. 8(a). [The inset in Fig. 8(a) also shows the hf levels connected by the four components, again assuming that the hfs of both the lower and upper levels is normal.] However, due to the low power of the laser diode we used at this wavelength and the inherent weakness of this transition, we were able only to see two of the four hf components in the saturated absorption spectrum. (The radiative transition probability from the upper to the lower level A_{ul} is 0.061×10^{8} s^{-1} at 761 nm, as opposed to 0.35×10^{8} s^{-1} at 775 nm and 0.29×10^{8} s^{-1} at 780 nm [23].)

The Doppler-limited spectrum shown in Fig. 8(a) was obtained by subtracting a scan of the diode laser power transmitted through the discharge cell when the discharge was on from a scan taken with the discharge off, but not normalized against the variation in the laser power across the scan. Since the laser power was only 20% less on the extreme high-frequency side than at the low-frequency side, we ignored this variation. We carried out a 14-parameter fit to this spectrum (independent positions, widths, and amplitudes for each of the four peaks, plus a background offset and slope). This fit, also shown in Fig. 8(a) together with the residuals (top trace), revealed that the Gaussian FWHM of the components is 1.68 ± 0.04 GHz, corresponding to a temperature of 690 ± 50 K in the discharge (assuming that the Lorentzian width is negligible compared to the Gaussian width). This Gaussian width (suitably modified for the different wavelengths) was used to determine the residual Doppler broadening of the saturated absorption spectra at 775 and 780 nm, as described above. For the situation shown in the inset of Fig. 8(a), where transitions are allowed from both lower F values to both upper F' values, the Burger-Ornstein-Dorgelo sum rule is insufficient to determine the expected relative intensities. Instead, we used the results of the quantum-mechanical calculation, valid for LS coupling, the results of which have been tabulated by White and Eliason [24]. The relative amplitudes of the a, b, c, and d hf transitions obtained using these tables is 1:9:5:1 (0.11:1.0:0.56:0.11), whereas the values obtained from the fit are 0.12:1.0:0.59:0.11. As can be seen, the agreement is excellent. From the fitted positions of the centers of the Gaussian profiles, we obtained independent value of the hfs splittings of the $^2P_{3/2}$ and $^2D_{3/2}$ states and the magnetic-dipole coupling constants A. In particular, we obtained the values $A(^2P_{3/2})=3018\pm50$ MHz and $A(^2D_{3/2})=1807\pm50$ MHz (the values given are averages from three different data scans). These values are in agreement with those shown in Table II, but are significantly less precise. This is perhaps not surprising, since the 2-GHz étalon used to linearize the spectra was not temperature stabilized, and also the widths of the Doppler-limited spectra are greater than 1 GHz. Indeed, we made some attempts to fit the Doppler-limited spectra at 780 and 775 nm (which were linearized with the temperature-stabilized 150-MHz étalon) and these fits resulted in comparable discrepancies with the hfs splittings and couplings obtained from the Doppler-free spectra. In addition, the laser scan was somewhat nonlinear (as noted above), suggesting that the frequency scan nonlinearities may also contribute to the imprecision of these data.

It is perhaps more enlightening to fit the Doppler-limited spectrum at 761 nm using the hfs coupling constants obtained at 775 and 780 nm. This fit is shown in Fig. 8(b); the experimental spectrum is the same as that shown in Fig. 8(a), while the fitted spectrum has the constraint that the relative positions of the four hf components are fixed to the values obtained using the A values for the $^2P_{3/2}$ and $^2D_{3/2}$ states given in Table II. This fit had 11 free parameters (four widths and amplitudes, a background offset and slope, and one frequency position). As can be seen, the agreement is very good; the difference between the experimental spectrum and the synthesized spectrum is nowhere greater than 5% of the maximum signal amplitude. Hence, considering this fit and the relative transition amplitudes, we conclude that our assignment of the F values given in Figs. 6 and 8 is correct and the hf coupling constants are as given in Table II.

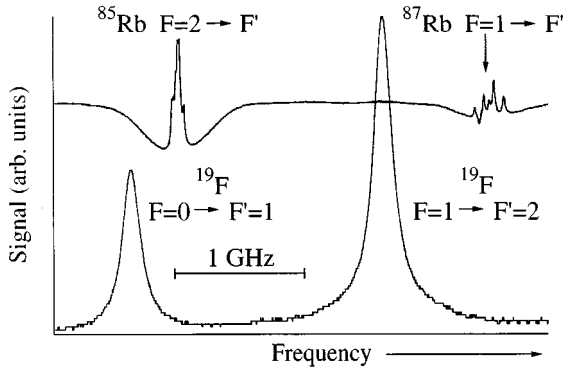

FIG. 9. Doppler-free spectra of the Rb $5s\ ^2S_{1/2}\rightarrow5p\ ^2P_{3/2}$ transition (upper trace) and the two strongest components of the ^{19}F $^2P_{1/2}\rightarrow{}^2D_{3/2}$ transition (lower trace) at 780 nm.

C. Absolute frequency of the $^2P_{1/2}(F=1)\rightarrow{}^2D_{3/2}(F=2)$ transition

The F $^2P_{1/2}\rightarrow{}^2D_{3/2}$ transition (12 817.0 cm^{-1}) is almost coincident with the Rb $5s\ ^2S_{1/2}\rightarrow5p\ ^2P_{3/2}$ D_2 resonance line (12 816.56 cm^{-1}) [14]. Indeed, we used the Rb D_2 absorption line as a marker to tune our external cavity diode laser to the vicinity of the F transition. Our Rb saturated absorption spectrometer was especially simple [11]; one of two probe beams interacts with a more intense counter-propagating pump beam (crossing angle 25 mrad) in a room-temperature Rb cell (Opthos Instruments). The Doppler-free absorption is then obtained by taking the difference signal between the absorptions of the two probe beams as detected by two photodiodes. Since the laser beam used in the Rb spectrometer originated from the laser intra-cavity beam splitter, whereas the beam for the F spectrometer came from the diffraction grating, we were, in principle, able to take Doppler-free spectra of both F and Rb simultaneously. However, our digitizing oscilloscope could only acquire two channels simultaneously; consequently, we had to alternate scans of the fluorine spectrum plus 150-MHz étalon fringes with scans of the rubidium spectrum and 150-MHz étalon fringes taken a few minutes apart. An example of such a scan is shown in Fig. 9. The upper spectrum shows the ^{85}Rb($F=2\rightarrow F'$) hf multiplet on the left and the ^{87}Rb($F=1\rightarrow F'$) hf multiplet on the right. Here F is the total angular momentum of the $5s\ ^2S_{1/2}$ Rb ground state and F' is the total angular momentum of the $5p\ ^2P_{3/2}$ Rb upper state.

TABLE III. Absolute frequency of the ^{19}F $^2P_{1/2}(F=1)\rightarrow{}^2D_{3/2}(F'=2)$ transition.

Transition or interval	Frequency (MHz)
(1) ^{87}Rb $^2S_{1/2}\rightarrow{}^2P_{3/2}(F=2\rightarrow F'=2)$, $(F=2\rightarrow F'=3)$ crossover[a]	384 227 981.8773±0.0055
(2) ^{87}Rb $^2P_{3/2}(F'=3,\ F'=2)$ interval[a]	266.650±0.009
(3) ^{87}Rb $^2S_{1/2}(F=2,\ F=1)$ interval[b]	6834.682 613±0.000 001
(4) ^{87}Rb $^2S_{1/2}(F=1)\rightarrow{}^2P_{3/2}(F'=2)$ transition $[(1)-\frac{1}{2}\times(2)+(3)]$	384 234 683.235±0.007
(5) ^{87}Rb $^2S_{1/2}(F=1)\rightarrow{}^2P_{3/2}(F'=2)$, ^{19}F $^2P_{1/2}(F=1)\rightarrow{}^2D_{3/2}(F'=2)$ interval[c]	961.2±7.0
(6) Correction for AOM downshift[c]	23.99±0.01
(7) ^{19}F $^2P_{1/2}(F=1)\rightarrow{}^2D_{3/2}(F'=2)$ frequency $[(4)-(5)-(6)]$	384 233 698.0±7.0

[a]Reference [25].
[b]Reference [13].
[c]This work.

The $(F'=1,2,3)$ components and their three crossovers are only partially resolved in the ^{85}Rb $^2S_{1/2}(F=2)\rightarrow{}^2P_{3/2}(F')$ transition, but close inspection of the ^{87}Rb $^2S_{1/2}(F=1)\rightarrow{}^2P_{3/2}(F')$ line reveals the $(F'=0,1,2)$ hf components and the three crossovers (the lowest-frequency crossover is inverted). The lower spectrum shows the two strongest components of the ^{19}F $^2P_{1/2}\rightarrow{}^2D_{3/2}$ Doppler-free spectrum: the $(F=0\rightarrow F'=1)$ on the left and the $(F=1\rightarrow F'=2)$ on the right.

From the Rb and F spectra, we were able to measure the apparent frequency separation between the ^{19}F $^2P_{1/2}(F=1)\rightarrow{}^2D_{3/2}(F'=2)$ and the ^{87}Rb $^2S_{1/2}(F=1)\rightarrow{}^2P_{3/2}(F'=2)$ (the highest-frequency hf component) transitions to be 961.2±7.0 MHz, with the Rb transition lying higher in frequency. The quoted error in the measurement (an average of four scans) is dominated by the uncertainty in the fit to the center of the F transition of width ~150 MHz and residual uncertainty in the drift rate of the 150-MHz étalon. To convert this measurement to an absolute frequency for the ^{19}F $^2P_{1/2}(F=1)\rightarrow{}^2D_{3/2}(F'=2)$ transition, we have taken advantage of recent measurements of the absolute frequency of the crossover between the $(F=2\rightarrow F'=2)$ and the $(F=2\rightarrow F'=3)$ component of the ^{87}Rb $^2S_{1/2}\rightarrow{}^2P_{3/2}$ transition and the hf splittings of the ^{87}Rb $5p\ {}^2P_{3/2}$ state [25] and the well-known hf splitting of the ^{87}Rb $5s\ {}^2S_{1/2}$ state [13]. Specifically, the frequency of the crossover between the $(F=2\rightarrow F'=2)$ and $(F=2\rightarrow F'=3)$ components of the ^{87}Rb $^2S_{1/2}\rightarrow{}^2P_{3/2}$ transition was measured to be 384 227 981.8773±0.0055 MHz and the ^{87}Rb $5p\ {}^2P_{3/2}(F'=3,\ F'=2)$ hyperfine splitting was measured as 266.650±0.009 MHz [25]. The ^{87}Rb $5s\ {}^2S_{1/2}(F=2,\ F=1)$ splitting has been measured by various methods as reported in Ref. [13] to be 6834.682 613 MHz, with an uncertainty of less than 1 Hz. Using these values, we calculated the absolute frequency of the ^{87}Rb $^2S_{1/2}(F=1)\rightarrow{}^2P_{3/2}(F'=2)$ transition (the highest-frequency hf component of the right-hand multiplet in Fig. 9) to be 384 234 683.235±0.007 MHz. To find the absolute frequency of the ^{19}F $^2P_{1/2}(F=1)\rightarrow{}^2D_{3/2}(F'=2)$ transition, we subtracted the interval 985.19±7.0 MHz, which is the sum of 961.2 MHz, the apparent frequency separation of the Rb and F features, and 23.99 MHz, one-half of the AOM frequency. In the F saturated absorption spectrometer, the pump light passes through the AOM and is downshifted relative to the laser by 47.98 MHz, but the probe beam is unshifted. The center of each saturated absorption resonance is observed when the laser is tuned so that atoms with a certain velocity observe both the pump and probe beams to have exactly the frequency corresponding to the spacing of the atomic levels. To satisfy this condition, the pump and probe beams must interact with atoms that are traveling toward the pump beam with a velocity component in that direction sufficient to Doppler-shift the laser frequency by 23.99 MHz. This Doppler-shift increases the frequency of the pump by 23.99 MHz, but decreases the frequency of the probe by the same amount, as observed in these atoms' rest frame. These atoms thus observe the pump and probe beam frequencies to be the same and equal to the resonance frequency when the laser is tuned 23.99 MHz higher in frequency than the resonance condition given by the energy-level spacing. On the other hand, there is no AOM in the Rb spectrometer and consequently the resonances are observed when the laser frequency matches the atomic energy spacing. Hence there is a frequency shift between the Rb and F spectra, which is not apparent in Fig. 9. One must thus subtract 23.99 MHz from our fluorine absorption frequency inferred from Fig. 9 to obtain the correct resonance frequency. Our final result for the frequency of the ^{19}F $^2P_{1/2}(F=1)\rightarrow{}^2D_{3/2}(F'=2)$ transition was thus 384 233 698.0±7.0 MHz. The full analysis is shown in Table III.

Using our measured value for the ^{19}F $^2P_{1/2}(F=1)\rightarrow{}^2D_{3/2}(F'=2)$ transition frequency and our values for the magnetic hfs coupling constants of the $^2P_{1/2}$ and $^2D_{3/2}$ states from Table II, we were also able to calculate the center of gravity of the $^2P_{1/2}\rightarrow{}^2D_{3/2}$ transition multiplet, for which we obtained the value of 384 232 739.5±8.0 MHz or 12 816.6246±0.0003 cm^{-1}. This value is in significant disagreement with that of Lidén [8], who gives a value of 12 816.643±0.003 cm^{-1} for this center of gravity frequency.

The difference between these two values is 0.018 cm^{-1}, some six times larger than Lidén's estimated uncertainty for his interferometric measurement of the transition wave number. Given the unambiguous nature of the data shown in Fig. 9, we are confident in the precision of our results. The most likely reason for the discrepancy of the two results is the fact that Lidén seriously underestimated the hfs splitting of the $^2P_{1/2}$ state (180±150 MHz versus our measurement of 1737.1±4.0 MHz) and, to a lesser extent, that of the $^2D_{3/2}$ state (3060±150 MHz versus our measurement of 3714.2 ±4.2 MHz). Obviously, such errors in the hfs splittings translate directly into an error in the inferred value of the center of gravity of a multiplet from a measured frequency of one of its components.

IV. CONCLUSION

We have carried out Doppler-free spectroscopy of excited states of atomic fluorine. This is the first time, to our knowledge, that high-resolution spectroscopy has been carried out on excited states of this atom. Our ability to carry out these experiments was largely determined by the efficiency of our excitation system for fluorine atoms, namely, collisions of fluorine atoms and molecules with internally excited helium atoms in a microwave discharge. Other recent papers have reported similar success in exciting atomic oxygen [1] and nitrogen [2], in which the efficient excitation of atomic species was attributed to a low-frequency rf discharge (≈30 MHz) system, with trace quantities of O_2 or N_2 in He. Our result suggests that the particulars of the discharge environment are relatively unimportant, provided that sufficient helium is present; excited atomic species are generated just as efficiently as 2.45 GHz as at 30 MHz. It should be pointed out, however, that since the F_2 bond dissociation energy is very much less than for N_2 and O_2, the comparison is not entirely valid. On the other hand, the advantage of lower dissociation energy in F_2 must be weighted against the fact that the lower state of the transitions reported in this work on F lie some 20 000 cm^{-1} higher in energy than the lower states used in the experiment on nitrogen [2] and 30 000 cm^{-1} higher than in the experiments on oxygen [1]. A more valid comparison would be for us to attempt to generate excited N and O atoms using our discharge system, which we have not yet done.

Hyperfine structure intervals for the three fine structure components of the $^{19}F\ 3s\ ^2P_J \rightarrow 3p\ ^2D_{J'}$ multiplet were measured, resulting in values for the hyperfine splittings and magnetic coupling constants of the upper and lower levels. The values for the hfs splittings we obtained are at least an order of magnitude more precise than values previously obtained using conventional spectroscopic techniques [8,9] and in some cases are significantly different from the previous reported values. We found the ordering of the hyperfine sublevels was normal (in contrast with the inverted fine structure), which has also been found in other studies on the hfs of the ground states of fluorine [6,26,27]. Generally, the hf splittings were similar in magnitude to the splittings measured for the $2p^5\ ^2P_{3/2}$ and $^2P_{1/2}$ states of the ground configuration of ^{19}F using mid-infrared diode laser spectroscopy [6] and electron paramagnetic resonance [26,27]. In addition, we have measured the natural linewidth of the $2p^4\ ^2P_J \rightarrow 2p^4 3p\ ^2D_{J'}$ transitions and found them to be in good general agreement with the value obtained from the radiative lifetimes of the upper and lower states [7,17]. Finally, we have measured the absolute frequency of the $^{19}F\ ^2P_{1/2}(F=1) \rightarrow {}^2D_{3/2}(F'=2)$ transition by exploiting its close spectral proximity to a recently measured secondary frequency standard in ^{87}Rb. From this the frequency of the center of gravity of the $^{19}F\ ^2P_{1/32} \rightarrow {}^2D_{3/2}$ multiplet was obtained and found to differ significantly from a previously reported value [8].

ACKNOWLEDGMENTS

We would like to thank Jeff Dunham for many discussions during the initial stages of this research program and also for his loan of a fluorine regulator. Jim Veale donated a hard-to-obtain diode laser at 761 nm. Charlie Conover, Robert Bluhm, and Mike Renn have provided valuable advice. We also acknowledge much assistance from Wallie Leung, Julie Rentz, Alex Sobel, and Josh Walton. Funding for these experiments has been provided by Colby College, a William and Flora Hewlett Foundation grant administered by the Research Corporation, and a grant from the Maine Experimental Program to Stimulate Competitive Research administered by the Maine Science and Technology Foundation under Grant No. MSTF 96-12N.

[1] G. M. Tino, L. Hollberg, A. Sasso, and M. Inguscio, Phys. Rev. Lett. **64**, 2999 (1990).
[2] M. de Angelis, M. Inguscio, L. Julien, F. Marin, A. Sasso, and G. M. Tino, Phys. Rev. A **44**, 5811 (1991).
[3] P. Cangiano, M. de Angelis, L. Gianfrani, G. Pesce, and A. Sasso, Phys. Rev. A **50**, 1082 (1994).
[4] L. Gianfrani, A. Sasso, G. M. Tino, and M. Inguscio, Opt. Commun. **78**, 158 (1990).
[5] A. C. Stanton and C. E. Kolb, J. Chem. Phys. **72**, 6637 (1980).
[6] G. A. Laguna and W. H. Beattie, Chem. Phys. Lett. **88**, 439 (1982).
[7] G. C. Herring, M. J. Dyer, L. E. Jusinski, and W. K. Bischel, Opt. Lett. **13**, 360 (1988), and references therein.
[8] K. Lidén, Ark. Fys. **1**, 229 (1949).
[9] L. O. Hocker, J. Opt. Soc. Am. **68**, 262 (1978).
[10] F. C. Fehsenfeld, K. M. Evenson, and H. P. Broida, Rev. Sci. Instrum. **36**, 294 (1965).
[11] K. B. MacAdam, A. Steinbach, and C. Wieman, Am. J. Phys. **60**, 1098 (1992).
[12] C. E. Wieman and L. Hollberg, Rev. Sci. Instrum. **62**, 1 (1991).
[13] E. Arimondo, M. Inguscio, and P. Violino, Rev. Mod. Phys. **49**, 31 (1977), and references therein.
[14] C. E. Moore, *Atomic Energy Levels*, Natl. Bur. Stand. (U.S.) Circ. No. 467 (U.S. GPO, Washington, DC, 1958).
[15] L. W. Parker and J. R. Holmes, Phys. Rev. **90**, 142 (1953).

[16] M. D. Levenson and S. S. Kano, *Introduction to Nonlinear Laser Spectroscopy*, revised ed. (Academic, San Diego, 1988), p. 98.
[17] E. H. Pinnington, D. J. G. Irwin, A. E. Livingston, and J. A. Kernahan, Can. J. Phys. **54**, 1014 (1976).
[18] H. G. Kuhn, *Atomic Spectra*, 1st ed. (Longmans, London, 1962), p. 386.
[19] C. Brechignac, R. Vetter, and P. R. Berman, Phys. Rev. A **17**, 1609 (1978).
[20] M. D. Levenson and S. S. Kano, *Introduction to Nonlinear Laser Spectroscopy* (Ref. [16]), p. 87.
[21] L. H. Domash, B. J. Feldman, and M. S. Feld, Phys. Rev. A **7**, 262 (1973), and references therein.
[22] I. I. Sobelman, *Atomic Spectra and Radiative Transitions*, 2nd ed. (Springer-Verlag, Berlin, 1992), p. 157.
[23] W. L. Wiese, M. W. Smith, and B. M. Glennon, *Atomic Transition Probabilities (Volume I Hydrogen Through Neon*), Natl. Bur. Stand. (U.S.) (U.S. GPO, Washington, DC, 1966).
[24] H. E. White and A. Y. Eliason, Phys. Rev. **44**, 753 (1933).
[25] J. Ye, S. Swartz, P. Junger, and J. L. Hall, Opt. Lett. **21**, 1280 (1996).
[26] H. E. Radford, V. W. Hughes, and V. Beltran-Lopez, Phys. Rev. **123**, 153 (1961).
[27] J. S. M. Harvey, Proc. R. Soc. London, Ser. A **285,** 581 (1965).